Journal of Materials Processing Tech. 341 (2025) 118862

Contents lists available at ScienceDirect

Journal of Materials Processing Tech.

journal homepage: www.elsevier.com/locate/jmatprotec

Research article

Effect of consumable stud microstructure on friction surfacing: Comparison between friction extruded and hot extruded AA2024 studs

Pietro Aspes [a,*], Zina Kallien [a,b], Lars Rath [a], Uceu Suhuddin [a], Benjamin Klusemann [a,b]

[a] Solid State Materials Processing, Institute of Material and Process Design, Helmholtz-Zentrum Hereon, Max–Planck-Straße 1, Geesthacht, 21502, Germany
[b] Institute for Production Technology and Systems, Leuphana University Lüneburg, Universitätsallee 1, Lüneburg, 21335, Germany

ARTICLE INFO

Keywords:
Solid state layer deposition
Friction extrusion
Microstructure
Hardness
Deposition behavior

ABSTRACT

Friction surfacing is a solid-state layer deposition process that shows high potential as a coating and an additive manufacturing technique for aluminum alloys. Avoiding high temperatures, it does not suffer common challenges of fusion-based techniques, such as hot cracking. Friction surfacing and other solid-state processes commonly use studs from conventional hot extrusion, which are characterized by long elongated grains. However, limited research focused on different consumable materials. In this study, friction surfacing is successfully employed for the first time on friction extruded AA2024 studs and compared to hot extruded ones with respect to process behavior and resulting deposit. Friction extrusion produces rods characterized by a refined grain structure, illustrating the effect of a different microstructure on the friction surfacing process. Despite a completely different initial microstructure, the analysis of the deposits showed similar ultra-fine grain sizes (1.4 μm). However, results show strong effects of the consumable stud microstructure on the FS process behavior as well as the resulting deposit geometry. The fine-grained friction extruded studs feature 80% higher stud consumption rate, but 15% lower bonded width compared to hot extruded studs. These findings are of high value to successfully adapt the deposition parameters in case different consumable materials are employed, considering the high recycling potential of friction extrusion.

1. Introduction

Modern materials processing approaches have to meet sustainability and environmental requirements, for instance, ensuring the ability to process recycled materials [1]. From this perspective, aluminum is a very important material in the worldwide industry, in particular in the transportation sector, where aluminum scrap is traded globally [2]. Several approaches for the energy-efficient solid-state recycling of aluminum chips are mentioned in literature for both conventional hot extrusion [3] as well as friction extrusion, a friction stir-based solid-state process [4,5]. While both benefit from less material loss and lower energy consumption [6], the latter has the potential to efficiently handle contamination and oxide formation due to the additional rotational shear component imposed on the feedstock material. Moreover, a special interest is given to solid-state techniques, which are more environmentally friendly and do not necessitate material fusion or heating, resulting in a lower energy input that is needed as well as less material loss [6].

Such solid-state approaches enable recycling and have the potential to handle bulk, powder, or chip materials. They are based on severe plastic deformation and lead to a high degree of dynamic recrystallization (DRX) [6] and, thus, a highly refined grain structure. Two main categories of solid-state processes can be identified: processes that extrude tubes, e.g., shear-assisted processing and extrusion [7], tubular channel angular pressing [8], parallel tubular channel angular pressing [9]; or processes that extrude wires and bars, e.g., equal channel angular pressing [10], high-pressure torsion extrusion [11], friction stir back extrusion [12], or friction extrusion [13].

Extensive efforts were taken by researchers to understand and optimize the resulting extrudate to ensure the original material properties which can be challenging for materials recycling [14,15]. In this regard, solid-state extrusion techniques offer high potential for materials production and properties improvement.

Along the listed processes, friction extrusion is a promising candidate, as it is capable of upcycling materials [16] and improving their properties [17], of achieving mechanical alloying [18], therefore providing the possibility to tailor the chemical composition of extrudates, i.e., creating unique materials, and to synthesize high-performance materials [19,20]. Friction extrusion produces a fully consolidated rod, which facilitates the possibility of re-processing the extrudate with

* Corresponding author.
E-mail address: pietro.aspes@hereon.de (P. Aspes).

https://doi.org/10.1016/j.jmatprotec.2025.118862
Received 17 December 2024; Received in revised form 28 March 2025; Accepted 14 April 2025
Available online 2 May 2025

Nomenclature

Abbreviations

AM	Additive manufacturing
AS	Advancing side
AVG	Average
BC	Bottom center
BC+6.5	Bottom center + 6.5 mm
BM	Base material
CB	Center bottom
CM	Center middle
CT	Center top
DRX	Dynamic recrystallization
EBSD	Electron backscatter diffraction
FE	Friction extruded
FL	Flash
FS	Friction surfacing
GOS	Grain orientation spread
HAGBD	High-angle grain boundary distance
HAZ	Heat-affected zone
IPF	Inverse pole figure
RS	Retreating side
TC	Top center
TE	Top edge
TMAZ	Thermo-mechanically affected zone

Symbols

A	Elongation at break
d	Deposit thickness
e_s	Nominal specific energy
F_z	Axial force
$\eta_{joining}$	Joining efficiency
P_t	Torsional power
P_z	Axial force power
r	Radius
r_c	Contact radius
R_m	Ultimate tensile strength
$R_{p0.2}$	Yield strength
T	Torque
v_{CR}	Consumption rate
v_{tr}	Travel speed
ω	Rotational speed
w	Deposit width

other deposition techniques to obtain coatings or manufacture different parts via additive manufacturing (AM). Additionally, friction extrusion can feature advantages to other recycling routes: it can work continuously, produce long lengths of wires, and can be easily scaled up for high-volume production [21].

However, up to now, a fundamental research gap lies in the knowledge on the processability of friction extruded (FE) materials in a subsequent processing step, such as AM. To the best knowledge of the authors, FE wires applications are reported only using fusion-based AM processes by Li et al. [4] and Carvalho et al. [5], which are both using a fusion-based AM process. Li et al. [4] presented the successful deposition of AA6061 wires with 1 mm and 2 mm diameter using wire arc additive manufacturing, obtaining mechanical properties for the build that were in the range of the AA6061 base material. Carvalho et al. [5] instead showed depositions of AA6082 wires with 1.6 mm diameter via gas tungsten arc welding. Single-layer depositions were successful, while multi-layer depositions suffered porosity defects, presenting an average density of 77%.

Moreover, when processing aluminum, fusion-based layer deposition approaches feature disadvantages related to the necessity of high process temperatures like alloying element volatilization, solidification cracking, and high residual stresses, making this technology challenging for a number of alloys and applications [22]. In contrast, friction stir-based solid-state layer deposition approaches operate at significantly lower temperatures and, therefore, have the potential to maintain the FE material advantages mentioned above.

Friction stir-based solid-state layer deposition techniques can also use different forms of consumable materials: (i) bulk in the form of plates, rods, and wires, (ii) powders, or (iii) chips. Processes using the latter two have the potential to directly recycle material instead of needing a pre-processing step but require a complex setup, such as friction screw extrusion additive manufacturing [23] or additive friction stir deposition with a dedicated auger to feed the material [24]. Processing bulk material consumables in the form of wires requires a complex tool as well, such as wire-based friction stir additive manufacturing [25] or joining processes with additional filler material like presented by Dong et al. [26] for friction stir welding. Regarding plates, these can be used for processes like friction stir additive manufacturing [27], but they have the disadvantage of needing surface machining after each layer deposition as well as a very large amount of unbounded material. Rods, on the other hand, are the most common consumable materials found in solid-state layer deposition techniques. In the recent literature, additive friction stir deposition represents the most prominent friction stir-based solid-state layer deposition technique, using either round-[28] or square-shaped consumable material [29] being fed through a hollow rotating tool. In this case, the bars are set into rotation together with the hollow tool and are pressed downwards, towards the substrate. However, also this technique necessitates a complex setup with a rotating spindle for the tool and a feeding mechanism for the rod and may necessitate a complex shape of tool surface featuring protrusions [30]. Other simpler approaches exist, which do not require a tool and can be executed with standard friction stir welding or milling machines, such as friction stir deposition or friction surfacing (FS) [31]. The first one used by [32] can be interpreted as FS without the movement of the substrate, i.e., it deposits the material locally at a single point, but follows the same principles as during the plasticizing phase of FS. To perform FS, a rotating stud material is pressed on a substrate with a defined axial force, which results in frictional heat at the materials' interface and deformation and plasticization of the stud tip. A relative translational movement enables the deposition of a continuous layer of the consumable material onto the substrate. The FS process parameters, i.e., rotational speed, axial force, and travel speed, depend on the materials to be deposited as they determine the energy input that is necessary for a successful FS layer deposition [33]. Having a simpler setup comes with drawbacks like less material deposition efficiency, i.e., only a part of the stud is deposited and the outer part is forming a process-characteristic flash; and deposits which are less consolidated, where the outer part is of the deposited layer is less bonded, which require post process removal by machining. Still, typically around 80% of the deposited material forms the defect-free structural bulk material [34].

Given its very simple setup, and easy application of FE studs, FS was chosen as friction stir-based solid-state layer deposition approach for the deposition of FE wires in this work. Using FE material means investigating the effect of a different consumable stud microstructure on the FS process. Addressing this knowledge gap is fundamental for later applications of FE materials such as recycled materials in general. This study presents a comprehensive analysis of solid-state layer deposition via FS using AA2024 consumable stud material obtained via conventional hot extrusion, as commercially available, and, for the first time, friction extrusion. Additionally, a solid solution treatment

stud of hot extruded material is included to compare FS performed on studs with a similar hardness but a different microstructure compared to the FE studs. The differences between the AA2024 consumable materials in terms of microstructure and mechanical properties on the FS layer deposition process are analyzed. In this regard, the study provides novel and extensive insight into the effect of the consumable stud initial microstructure on the FS deposition behavior as well as the resulting deposit's characteristics in terms of geometry and microstructure. Finally, an assessment of the transferability of FS process parameters from conventional to FE materials is discussed. By doing so, the authors demonstrate the feasibility of processing FE studs via FS, stimulating further investigations on (recycled) materials with tailored microstructures and/or compositions.

2. Materials and methods

The FS experiments were conducted on a friction welding machine (RAS, Henry Loitz Robotik, Germany), which allows axial forces up to 60 kN, rotational speeds up to 6000 rpm and torques up to 200 Nm, collecting process data (i.e., axial force, rotational speed, torque, and vertical displacement of the stud) at a frequency of 100 Hz. The recorded log files from the RAS machine are used to assess the process behavior during the deposition. The experiments have been conducted in force control mode at room temperature.

The substrates were AA2024-T3511 (8 mm thickness) with a surface manually ground with P100 grinding paper and degreased. A backing plate of AA7050 (8 mm thickness) was used between the substrate and the machine table.

The consumable stud material used in this study was AA2024 (13 mm diameter), where two different processing approaches were used: friction extrusion and conventional hot extrusion (commercially available). A schematic of both processes is shown in Fig. 1.

The FS process parameters were adapted from Hoffmann et al. [35] and all depositions were carried out with 2500 rpm rotational speed, 3 kN axial force and 5 mm/s travel speed. The achievable layer lengths varied between 70 and 85 mm, according to the consumption rate of each stud.

The FE rods used for machining FS consumable stud material were manufactured on a special-purpose friction extrusion machine (FE100, Bond Technologies, USA). As feedstock, AA2024-T3511 rods of 50 mm diameter were employed and extruded at a rotational speed of 90 rpm, a constant force of 300 kN, using a featureless flat die with a 14 mm central hole. The microstructure of the respective extrudate, Fig. 1b is characterized by elongated grains in the center, homogeneously refined and equiaxed grains along the edge, and a transition zone between those two regions where grain shape and size shift from one characteristic to the other, representing a typical feature of FE rods [36]. For further details on the friction extrusion process and its characteristic microstructure, the interested reader is referred for instance to [37]. The FE rod was machined to a diameter of 13 mm, to get the proper cylindricity of the studs while keeping as much fine-grained material from the outer part as possible, which represents one characteristic difference to conventional hot extrusion. The hot extruded consumable material is shown in Fig. 1d and is characterized by elongated grains across the whole radius.

The composition of the AA2024 consumable material was obtained via optical emission spectroscopy[1] for conventionally hot extruded and FE material, which is summarized in Table 1, respectively.

For the FS process analysis, AA2024 stud materials from both extrusion processes were used, as well as hot extruded AA2024 material solid solutionized prior to FS layer deposition. Being a precipitation-hardenable alloy, the heat treatment on the AA2024 consumable material leads to differences in mechanical properties, such as base materials' hardness.[2] This allows to additionally investigate how FS is affected by the mechanical properties, keeping the same chemical composition and grain structure. An overview of all consumable materials is given in Table 2. For all consumable materials, the FS process behavior as well as appearance and geometry of the resulting FS deposits were investigated.

Table 1
Optical emission spectroscopy data of AA2024-T3 (conventional, hot extruded) and AA2024 (friction extruded) in wt.%.

Consumable	Si	Fe	Cu	Mn	Mg	Cr	Ni	Zn	Ti	Sn	Al
Hot extruded	0.33	0.26	4.1	0.68	1.6	0.01	0.01	0.05	0.06	0.02	bal.
Friction extruded	0.11	0.21	4.2	0.76	1.4	0.07	0.01	0.01	0.01	<0.01	bal.

Table 2
Overview of consumable materials and respective heat treatment used for investigation of friction surfacing process behavior.

Label	Description
COM-2024-T3	conventional hot extruded AA2024-T3 'as-received'.
COM-2024-SS	conventional hot extruded AA2024-T3 solid solution treated with 30 min at 495 °C in salts bath followed by water quenching.
FE-2024	friction extruded AA2024.

Transverse cross-sections were cut from the deposited layers at 40 mm from the beginning of the deposition length in order to analyze the deposits with perspective to deposit geometry (thickness and width), bonding to substrate (bonded width) as well as microstructure. In addition, the remaining consumable studs after FS layer deposition were also analyzed in terms of microstructure. The samples were embedded and ground using grinding papers of P320-P800-P1200-P2000-P4000 for sixty seconds each, and polished using 1 μm diamond suspension for four minutes.

For geometrical measurements, micrographs before and after etching obtained via light-optical microscopes (VHX-6000, Keyence, Germany and Leica DMi8, Leica Microsystems, Germany) were used. Etching was conducted using the electrolytic technique (Barker's solution with 15.0 V, 60 s of exposure).

The specimens were subjected to an in-depth microstructural analysis to understand the effect of consumable stud microstructure on FS deposits. This analysis was performed via electron backscatter diffraction (EBSD) using an EDAX EBSD detector (Ametek, USA) mounted on a FEI Quanta 650 field-emission scanning electron microscope (Thermo Fisher Scientific, USA) after an additional sample preparation step of vibratory polishing with colloidal silica. The EBSD parameters were 15.0 kV, working distance of 15–20 mm, step size of 0.3–0.05 μm, at several magnifications, according to the grain size.

The FS deposits were scanned in five regions, Fig. 2a: in the center of the layer, at the bottom at the layer-to-substrate interface (CB), in the middle (CM) and at the top (CT) along the height; in the middle of the layer at advancing side (AS) and retreating side (RS). RS is the side of the deposit where the stud rotation opposes the deposition direction, and AS is where the rotation matches the deposition direction. The RS tends to show a wider unbonded edge compared to AS [39]. The consumed FS studs, showing the process-typical flash, were also scanned in five regions, Fig. 2b. Two scans were taken at the top for reference of the unprocessed base material (BM), at the center (radius = 0 mm, TC), and at the edge (radius = 6.5 mm, TE)[3]. Two scans were taken in the bottom zone of the stud: at the center (at radius = 0 mm, BC) and at

[1] Analysis carried out by Materia Services GmbH, Germany.

[2] Except for the solid solution heat treatment BM, one week of natural aging was ensured before performing any process or testing after FS. This time was sufficiently long to allow the formation of precipitates and to reach a hardness plateau [38].

[3] This position ensured that the analyzed grain structure was not affected by the process.

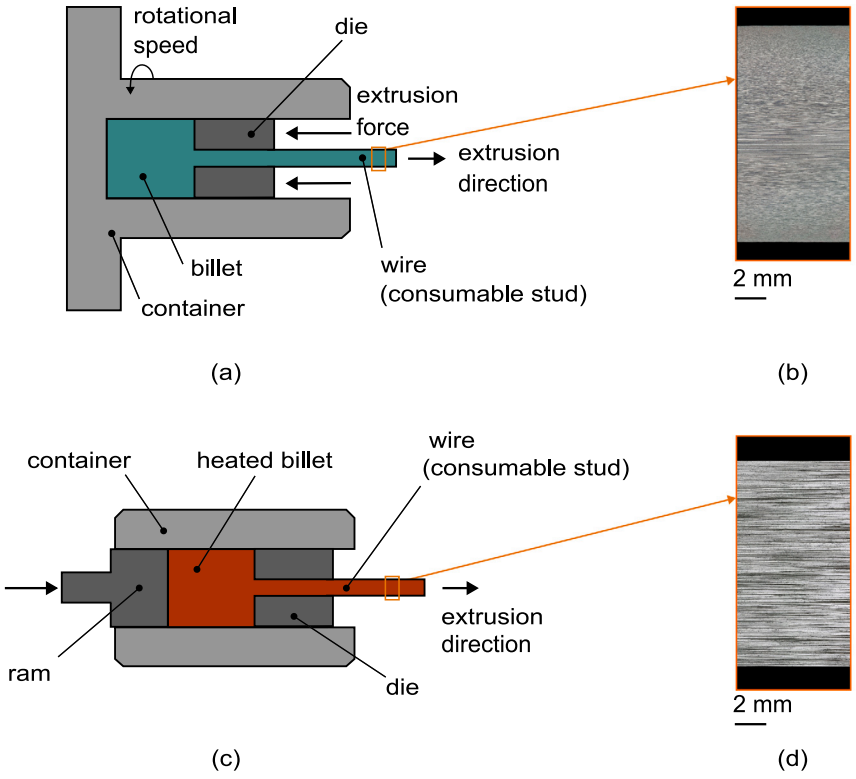

Fig. 1. Friction extrusion: (a) process schematic, (b) longitudinal cross-section of the wire as extruded (prior to machining, 14 mm diameter). The friction extruded rod elongated grain region is approximately 3.5 mm wide. Hot extrusion: (c) process schematic, (d) longitudinal cross-section of the wire (13 mm diameter).

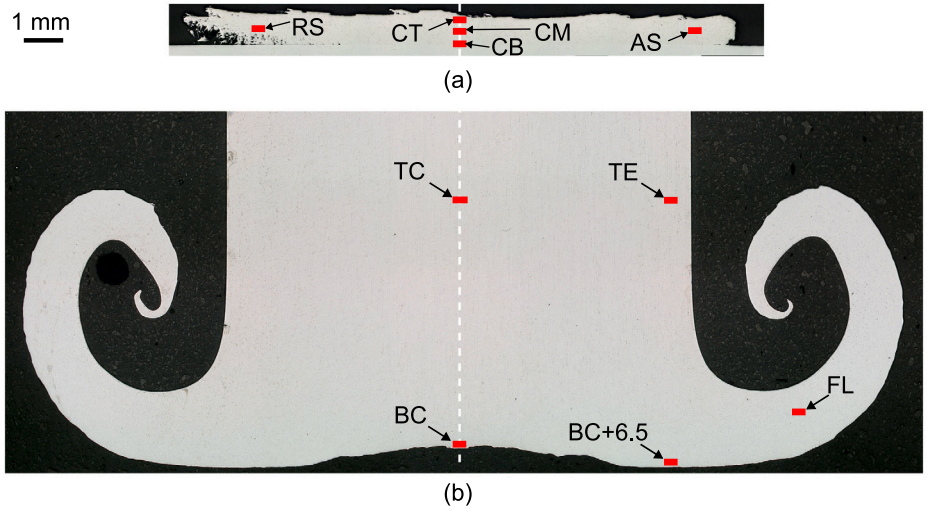

Fig. 2. Analyzed EBSD regions within (a) friction surfacing deposits: retreating side (RS), center top (CT), center middle (CM), center bottom (CB), advancing side (AS). Analyzed EBSD regions within (b) FS studs: top center (TC), top edge (TE), bottom center (BC), bottom center + 6.5 mm towards the edge of the stud (BC+6.5), flash (FL). The reference images used represent COM-2024-T3 layer (a) and the corresponding consumed stud (b).

a radius distance equal to the stud radius (at radius 6.5 mm, BC+6.5). The last position scanned was in the flash material (FL). The collected data was analyzed with the OIM Software.

To analyze the microstructure evolution, the assessment of the long elongated grains in the regions characterized by them (TC and TE of COM-2024-T3 and COM-2024-SS, and TC of FE-2024) has been performed using a minimum grain size of 1000 data points, to exclude small grains from the calculation.

In these cases, the horizontal intercept method was employed to collect the high-angle grain boundary distance (HAGBD) of long elongated grains along the extrusion direction, while for the other regions with equiaxed grains, the equivalent diameter method was used. Recrystallization was also investigated using the grain orientation spread (GOS), looking at misorientation values below 2° and 5°. These threshold values are commonly used to distinguish strain-free recrystallized grains from recrystallized grains that were subjected to small strains [40,41].

Micro-hardness measurements were performed with an automated hardness testing machine (Durascan 70 G5, EMCO-TEST Prüfmaschinen, Austria) on both the deposited layers and the studs. The Vickers indenter had a 136° opening angle, and the parameters used were HV0.1 at 10 s holding time, with a point spacing of 0.2 mm and 0.1 mm in width and thickness, respectively, for the layers; and an

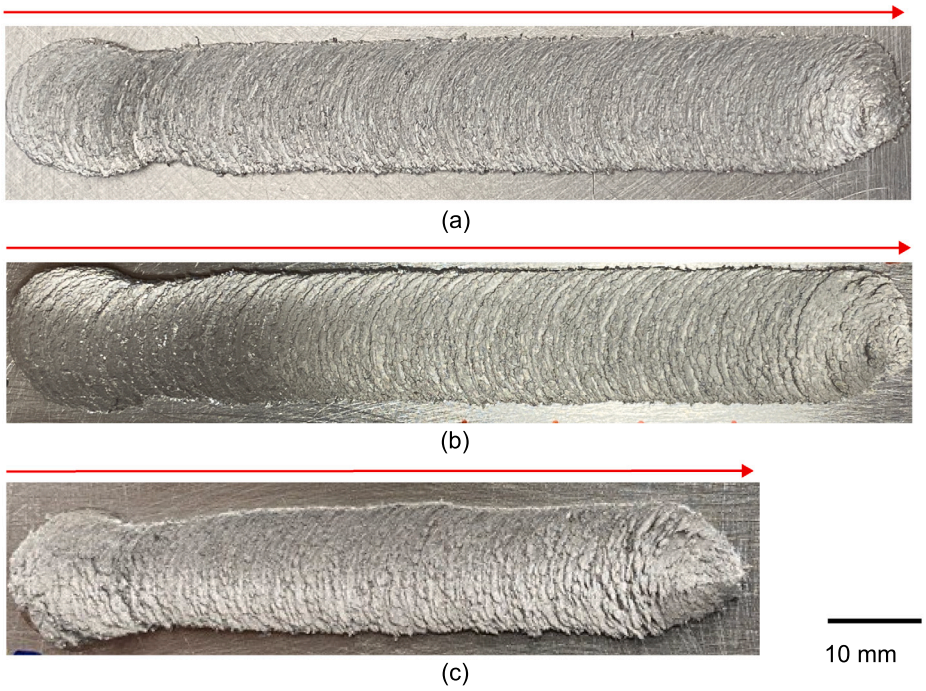

Fig. 3. Top view of friction surfacing depositions: (a) COM-2024-T3, (b) COM-2024-SS, (c) FE-2024. The arrow represents the advancing side and points from the beginning to the end of the deposition process. Both COM-2024 studs lead to a slightly more homogeneous deposition along the whole deposition length compared to FE-2024.

equidistant point spacing of 0.3 mm for the studs. Considering the studs' symmetry, hardness measurements were taken on half of each specimen. BM transverse cross-sections were tested following sample preparation with a single line with a distance of 0.4 mm between each point along the diameter.

In addition, a further indentation testing machine (i3D BVR, Imprintec GmbH, Germany) was employed to collect data about the plastic material behavior of the consumable stud materials by analyzing the profile of the indentation, following the DIN SPEC 4864 standard. BM longitudinal cross-sections of all deposited studs were tested. The standard indenter Type-B (spherical shaped with a radius of 100 μm) was used, the load was 5 kg and the material card "Al-unverified" was selected for the calculation of the stress–strain curves. For more information on this testing method, the interested reader is referred to [42].

3. Results and discussion

3.1. Friction surfacing process behavior

The process behavior was analyzed with respect to axial force, torque and vertical displacement that were recorded during the deposition of the different studs. From these, the stud consumption rate and nominal specific energy were calculated to further assess the difference in terms of process behavior between different consumable materials. A steady state of the process can be recognized by a constant force, a constant torque, and a linear vertical displacement, i.e., feeding, of the stud during the deposition, which typically results in a homogeneous appearance of the deposited layer. Fig. 3 shows the appearance of the FS depositions. The COM-2024-T3 and COM-2024-SS are homogeneous along the whole deposition length. In contrast, the first part of the FE-2024 deposit presents a slight increase in width and decrease in thickness, which are stabilizing in the second part. Another indicator of a stable process with uniform deposition is the process-typical flash, which is visible in the studs' cross-sections shown in Fig. 4. The flashes of conventionally extruded material appears to be more circular, while the one of the FE stud features a more irregular shape.

Table 3
Friction surfacing process average torque and consumption rate of the stud during deposition (steady-state conditions) and hardness of the respective consumable stud base material.

Process	Average torque, (Nm)	Average consumption rate, (mm/s)	BM hardness, (HV0.1)
COM-2024-T3	11.48	1.03	146
COM-2024-SS	11.36	1.02	107
FE-2024	11.36	1.87	102

Calculating the stud consumption rate (v_{CR}) gives insight into the amount of material that gets processed per unit of time during the process. It is obtained by the ratio of the total stud vertical displacement (S_z) over time (t) during steady state conditions: $v_{CR} = \frac{\Delta S_z}{\Delta t}$. Table 3 summarizes the average processes torque, the consumption rate and the measured BM hardness for the different AA2024 consumable studs, respectively. The conventionally extruded studs feature a lower stud consumption rate than the FE ones. This is further investigated in Section 3.4 considering the mechanical properties of the respective stud BMs.

The energy requirement of the FS processes was also calculated, according to the nominal specific energy. This is defined as the ratio between the power introduced during the process per consumed stud material volume [33]:

$$e_s = \frac{P_t + P_z}{\pi \cdot r^2 \cdot v_{CR}} = \frac{2 \cdot \pi \cdot \omega \cdot T + F_z \cdot v_{CR}}{\pi \cdot r^2 \cdot v_{CR}}. \quad (1)$$

The powers P_t and P_z are the torsional and the axial force power, respectively. The first depends on the rotational speed ω and torque T; the latter on axial force F_z and the stud consumption rate v_{CR}. The value r represents the radius of the consumable stud. The as-received material, COM-2024-T3, featured a higher nominal specific energy (22 J/mm^3) compared to the FE-2024 (12 J/mm^3).

From the analyses of the process data recorded by the welding equipment, the consumable materials investigated present differences in terms of the deposition behavior. At constant FS process parameters,

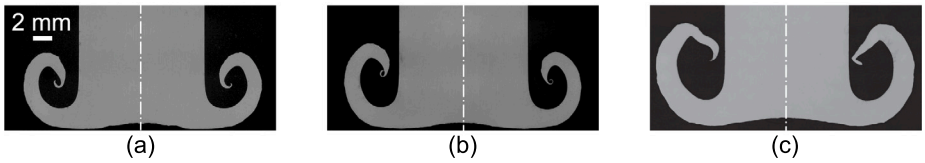

Fig. 4. Light-optical micrographs of stud cross-sections after the friction surfacing deposition process: (a) COM-2024-T3, (b) COM-2024-SS, (c) FE-2024. The FE-2024 stud shows a slightly more irregular flash shape compared to the other two studs.

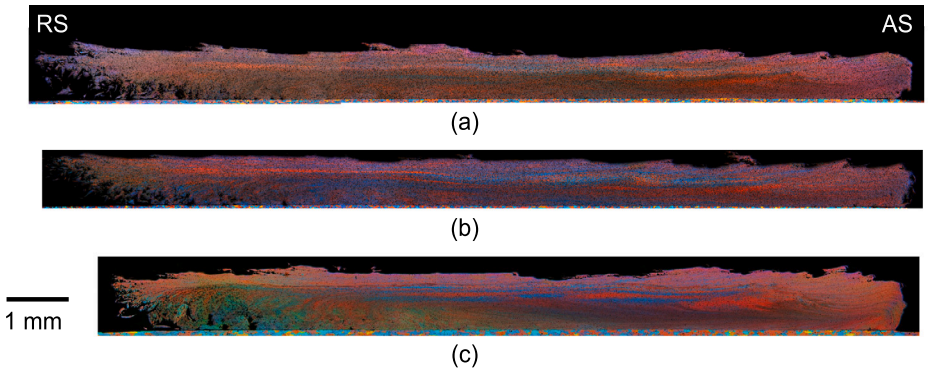

Fig. 5. Light-optical micrographs of transverse cross-sections of friction surfacing depositions: (a) COM-2024-T3, (b) COM-2024-SS, (c) FE-2024.

the FE stud features a slightly less homogeneous deposition at a higher stud consumption and requires less energy to be deposited.

3.2. Investigation of friction surfacing deposits

3.2.1. Deposit geometry

Fig. 5 shows the cross-sections of the deposits and Table 4 summarizes the characteristic values obtained. The analysis showed that the deposition from the FE stud features a slightly thicker and narrower deposit. This is a consequence of the different stud consumption rates: the material input per unit of time is higher for the FE stud compared to the as-received conventional studs. The FE deposit is also characterized by a narrower bonded width and lower joining efficiency[4] [43].

To improve the understanding of the resulting deposit geometries for FE and conventional consumable stud material, the assumed contact radius (r_c) has been calculated [44]:

$$r_c = \sqrt{\frac{d \cdot w \cdot v_{TR}}{\pi \cdot v_{CR}}}, \tag{2}$$

where d is the deposit thickness, w the deposit width, v_{TR} the substrate transverse speed and v_{CR} the stud consumption rate. This approach allows to assess the area below the consumable stud that is in direct contact with the substrate [44]. FE and conventional studs feature discrepancies in the contact radius, Table 4. The conventionally extruded consumable material (COM-AA2024-T3) presents a larger assumed contact area, which can be related to higher efficiency in material transfer from the stud to the deposit during the process and less material loss due to flash formation.

3.2.2. Microstructure

Etched micrographs of the deposits' cross-sections are shown in Fig. 5. All of the depositions feature FS-typical fine grains, irrespectively of the initial stud material, BM hardness and process behavior. The center is characterized by bands of material parallel to the substrate surface, indicative of material flow. At the outer part on the AS vortexes are visible, while the outer part on the RS is characterized by local defects and voids. These deposit characteristics are particular to FS layers [31]. As mentioned in the introduction, machining the FS layers is a common practice to achieve a good surface finish, where typically 80% of the deposited material can be used.

A more detailed analysis has been conducted via EBSD in the selected positions in Fig. 2. All EBSD results for the deposits are summarized in Fig. 6 and the inverse pole figure (IPF) maps taken for the analysis can be found in Appendix A. The deposits feature smaller average grain sizes at the center top and center bottom, but coarser grains at center middle, representing a characteristic feature of FS [45]. This observation can be attributed to a higher cooling rate at the substrate-to-deposition interface and a higher strain rate at the deposition-to-stud interface during the FS process. The average grain sizes at AS and RS are comparable with the bottom and top scans (CT and CB in Fig. 6).

Regarding these positions, literature reports both similar and contrasting results. Some studies show comparable grain sizes for AS and RS [46], and other larger sizes for AS compared to RS [47]. A possible explanation for the discrepancy between this study and the previous one is the smaller diameter of consumable stud materials of this work compared to those commonly applied in the literature. The reduced stud dimension leads to a smaller thickness and width of the depositions, which results in less pronounced thermal gradients along the deposit. Therefore, cooling occurs at a similar rate across the whole deposit, leading to fewer differences between the grain sizes at the top and the edges.

3.2.3. Hardness

The micro-hardness measurements for the FS deposits of this study show the highest hardness' at the top surface of deposits, and the lowest values in the center, Fig. 7, which is in accordance with the literature [35]. It is known that precipitation hardening is the main strengthening mechanism for this aluminum alloy [48]. The precipitates' size and distribution dominate the hardness of the layers [49], and it was found that fewer and coarser precipitates are present in low hardness regions as a consequence of more heat and lower cooling rates. Thicker deposits experience slower cooling [43], which is assumed to overage the center and bottom regions of the layer. During

[4] The joining efficiency, $\eta_{joining}$, was obtained by the ratio of bonded width over deposition width.

Table 4
Friction surfacing deposition measurements of COM-2024-T3, COM-2024-SS, FE-2024, including joining efficiency and the calculated assumed contact radius.

Sample	Width, (mm)	Bonded width, (mm)	Height, (mm)	$\eta_{joining}$	Area, (mm^2)	r_c (mm)
COM-2024-T3	13.85	9.35	0.78	68%	9.98	4.10
COM-2024-SS	13.71	9.75	0.71	71%	9.35	3.90
FE-2024	12.38	7.93	0.85	64%	10.64	2.99

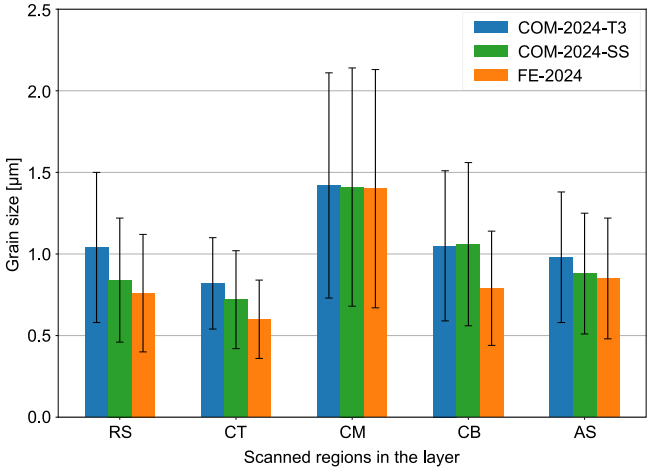

Fig. 6. Average grain size with 1 standard deviation error bars for COM-2024-T3, COM-2024-SS and FE-2024 deposits. Five positions, see Fig. 2a, were investigated via EBSD: advancing side (AS), center top (CT), center middle (CM), center bottom (CB), and retreating side (RS). The corresponding inverse pole figure maps are shown in Appendix A.

FS layer formation, the different regions form in a different order [50]: the center and the bottom of the layer are deposited first and the top is formed at the rear edge of the stud. This means the top part does not experience further heating or consolidation by the stud and can quickly be cooled by the ambient air, while the center and the bottom experience a longer heating and are cooled by convection through the substrate. This results in a slightly higher hardness value at the top, i.e., less overaging, compared to the rest deposit.

Comparing the HV maps of the stud configurations, Fig. 7, differences can be seen. The deposit FE-2024 (Fig. 7c) presents a lower hardness than the commercially hot extruded samples (Fig. 7a,b). As mentioned above, this can be justified by the layer being thicker. Therefore, it is assumed that hardness differences result from the different geometry of the deposits and not the different BM microstructure.

3.3. Investigation of consumed friction surfacing studs

3.3.1. Microstructure

Fig. 8 shows the studs' IPF maps and the average grain sizes after processing, according to positions shown in Fig. 2b. The black regions of the IPF maps represent unindexed and low-quality points with a confidence index of less than 0.2 that have not been taken into account.[5] The analysis of consumed FS studs is barely faced in the literature but can help to understand the microstructure evolution during the FS deposition process, which affects the resulting deposit's microstructure and properties. According to Suhuddin et al. [51], the stud material can be differentiated in the following zones: the bottom part that leads to the deposit is defined as the "friction zone", the lateral flash regions feature a "V" shape and are defined as the thermo-mechanically affected zone (TMAZ), and the rest of the stud is considered unaffected base material. These regions are shown in Fig. 10d with the addition of a heat-affected zone (HAZ). COM-2024-T3 and COM-2024-SS BM have elongated grains across the whole radius (TC and TE), while the FE BM features a bimodal microstructure (elongated and equiaxed grains) at the top center (TC). FE consumable material features smaller HAGBD in the top center (TC) and refined and equiaxed grains at the edge (TE), while the conventionally extruded material shows larger elongated grains across the whole radius.

The scans at the tip of the consumed FS studs (BC and BC+6.5, Fig. 8) in the friction zone, show that the microstructure gets significantly refined with respect to the BM. This is in agreement with literature findings, which show that aluminum studs undergo continuous and discontinuous dynamic recrystallization during the FS process [51,52].

A slight grain refinement is observable within the flash of samples COM-2024-T3 and COM-2024-SS compared to the BM, see Fig. 8. This is in accordance with the findings of Santiagu et al. [53], showing a small grain refinement in this region for Inconel 718, which indicates that this is a characteristic of FS consumable stud flash formation, independent of the specific alloy. It is assumed that the material in the TMAZ of the stud is subjected to low mechanical stresses and temperatures, as shown by the simulation of Pirhayati et al. [54], and is mainly bent away from the friction zone. This condition would be enough to refine very large grains of COM-2024-T3 and COM-2024-SS. The FE BM presents already refined grains in the outer parts of the stud, see top edge scan in Fig. 8, therefore, the formed flash material displays an average grain size similar to the respective BM previously refined via friction extrusion.

The above findings are further confirmed when considering the GOS values lower than 2° and 5°, see Fig. 9. The scans performed within the flash feature values very similar to top edge (TE) scans for the FE studs, and higher values for COM-2024-T3, confirming that a refinement is occurring for the latter. High GOS values can be found in bottom regions (BC and BC+6.5), where the material was subjected to DRX. When comparing GOS below 5° of these regions, they are almost the same for the studs analyzed, which further proves the local grain refinement by DRX.

3.3.2. Studs mechanical properties

The consumed studs' hardness maps are shown in Fig. 10. Considering the BM hardness in the top region of the studs as a reference, a decrease in hardness typically indicates the onset of the HAZ, see, for instance, COM-2024-T3 in Fig. 10a.

Although the hardness of the initial AA2024 consumable studs investigated in this study was different, all studs show a very similar hardness in the bottom region close to the edge of the sample. The hardness in this region is in the range of 120–130 HV0.1. As mentioned in the previous section, the hardness is mainly affected by the precipitates [48,49]. Considering also the similar average grain size results within the friction zone of all consumed studs, shown in Section 3.3.1, this indicates that a similar microstructure is achieved in this region for the different FS studs. However, it is important to consider that the region showing a refined microstructure is relatively small, as it can be seen by the IPF maps, Fig. 8a.

In addition to hardness mapping, the plastic material properties were determined for the different stud base materials via the Imprintec

[5] Edge rounding of samples cannot be avoided during sample preparation and often, in addition with particles and secondary phases, leads to low confidence index regions.

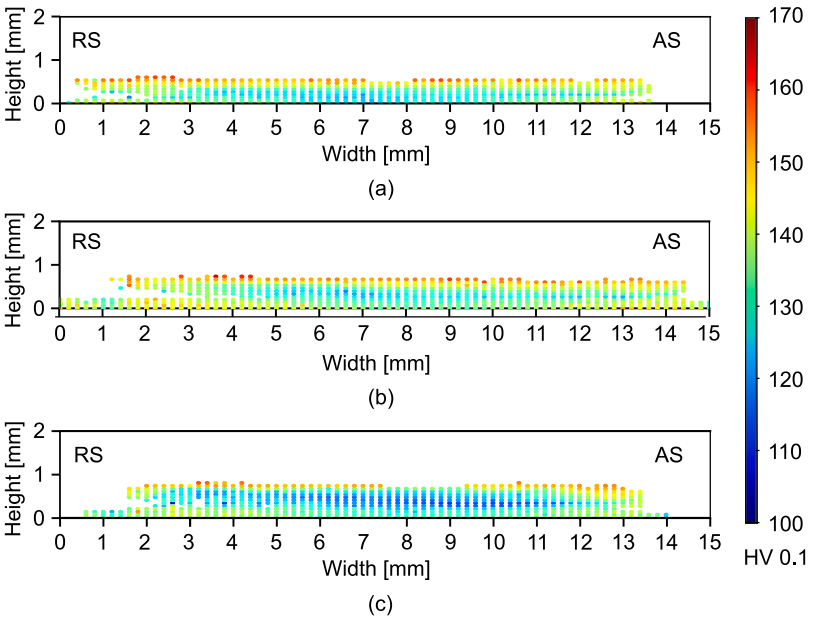

Fig. 7. Hardness map of transverse cross-sections from friction surfacing depositions: (a) COM-2024-T3, (b) COM-2024-SS and (c) FE-2024. The point spacing between indentations is 0.2 mm along the width and 0.1 along the thickness.

indentation method, Fig. 11. The base materials of COM-2024-SS and FE-2024 show a very similar hardness, Table 3, have a similar elongation at break (A), but, based on this indentation method, it is indicated that FE-2024 shows a slightly lower yield stress ($R_{p0.2}$) and ultimate tensile strength. In comparison to COM-2024-T3, both present lower $R_{p0.2}$ and R_m, but higher A. Exemplary indentation profiles can be found in Appendix B.

3.4. Correlation of consumable stud properties with resulting friction surfacing deposit

As shown before, the consumable stud BM microstructure and properties cause a significantly different FS deposition behavior at constant process parameters, resulting in slightly different deposit geometries. The processing during FS leads to a grain refinement from BM to stud tip to deposit. The BM grain sizes between the different studs are different, but once they advance from the top of the stud to the friction zone, the onset of DRX refines the grain structure, leading to similar grain sizes and hardness at the stud tip. The same applies to the resulting deposits, where the average grain size is similar and the differences in hardness are assumed to be caused by the geometry rather than different microstructure formation mechanisms during the process. A general refinement, occurring from BM to stud tip, and from stud tip to deposit was observed and is in agreement with other FS studies for different materials [48,53].

Unless the alloy composition and hardness might be similar, FS process behavior can be significantly different for the different stud BM microstructures. This study showed that not only the consumable material's hardness determines the FS process behavior,[6] but also the microstructure plays a vital role. Section 3.1 showed that COM-2024-SS and FE-2024 (which feature a very similar BM hardness) lead to different process behavior with different deposit geometries, where the conventionally hot extruded alloy presented a slightly more stable and homogeneous deposition, and a lower consumption rate. It is assumed that this occurs because of a different high-temperature mechanical behavior of the refined grains in the outer region of the FE-2024 stud.

Section 3.3.2 further investigated the mechanical properties. It is shown for samples COM-2024-SS and FE-2024 (which feature similar BM hardness), that macroscopically the refined grains do slightly affect R_m, and $R_{p0.2}$ at room temperature. In addition, literature shows that at the microscopic level, refined grains produced by a solid-state process can present a different deformation mechanism and behavior. For instance, in equal channel angular pressing, grain boundary sliding was found to occur [55]. Also, changes in fracture mechanisms have been observed when comparing AA7475 in the rolled, i.e., coarser grains, and friction stir processed, i.e., fine-grained microstructure, condition [56]. In general, for force-controlled FS processes, softer materials tend to show a higher stud consumption. However, the material strength at FS process temperature is affected by various aspects, e.g., composition or distribution and size of strengthening particles. For instance, Hanke and dos Santos [33] observed differences in process behavior for different aluminum alloys due to their different chemical composition. In addition, the temper state plays a huge role as it significantly influences the mechanical properties. Different tempers of AA2011 were investigated for friction stir deposition [57], where AA2011-O required lower feeding rates and rotational speed than AA2011-T6 because of its lower strength.

However, it is important to note that in this study the microstructure analyses, as well as the mechanical testing of the deposits and the consumed studs, were performed at room temperature. The FS process, instead, is highly dynamic and acts at elevated temperatures and stresses. At these working conditions, it is assumed that the deformation behavior and microstructure differences of long elongated and refined grains of COM-2024-SS and FE-2024, respectively, play a more significant role, affecting the mechanical properties and thus the whole process behavior during FS. In fact, at elevated temperatures, such fine-grained microstructure achieved by FS, shows different deformation behavior compared to the respective base material with coarser microstructure [58].

In this study, the FS process behavior is further analyzed in terms of energy consumption, geometry and contact radius. The calculated energy requirement is dependent on the consumption rate, which drops in case of the refined microstructure of the FE consumable material, which

[6] For completeness, additional experiments were performed for AA2024-T4 and over-aged condition of conventional AA2024-T3, Appendix C. The T4 temper state showed a deposition behavior very similar to the T3 condition. The over-aged condition did not show a homogeneous deposition behavior. For brevity, these experiments were not included in the main part of this article.

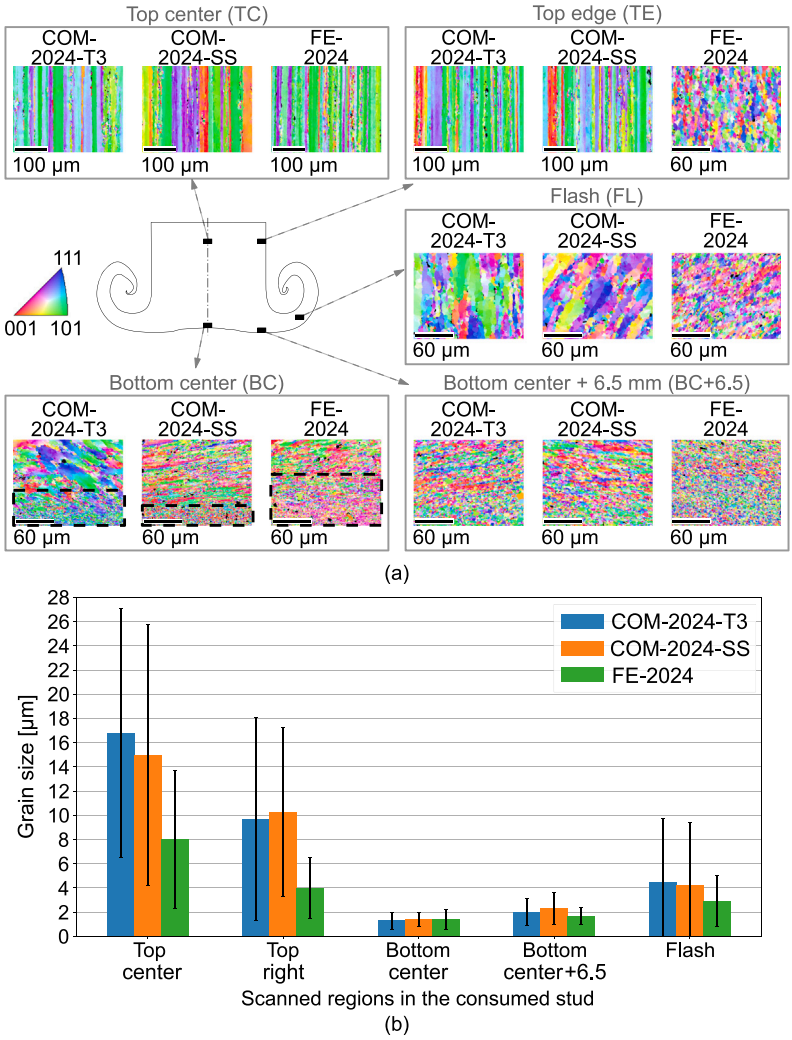

Fig. 8. (a) Inverse pole figure maps of EBSD scans of COM-2024-T3, COM-2024-SS, FE-2024 studs after friction surfacing, according to positions in Fig. 2b: top center (TC), top edge (TE), bottom center (BC), bottom center +6.5 mm (BC+6.5), flash (FL). Analyzed positions of the bottom center scans are defined by black dashed lines in the respective IPF maps. (b) Average grain size with 1 standard deviation error bars for scans of COM-2024-T3, COM-2024-SS and FE-2024 studs at different positions. Grain sizes of top center of all samples, and top right of COM-2024-T3 and COM-2024-SS were calculated as high angle grain boundary distance.

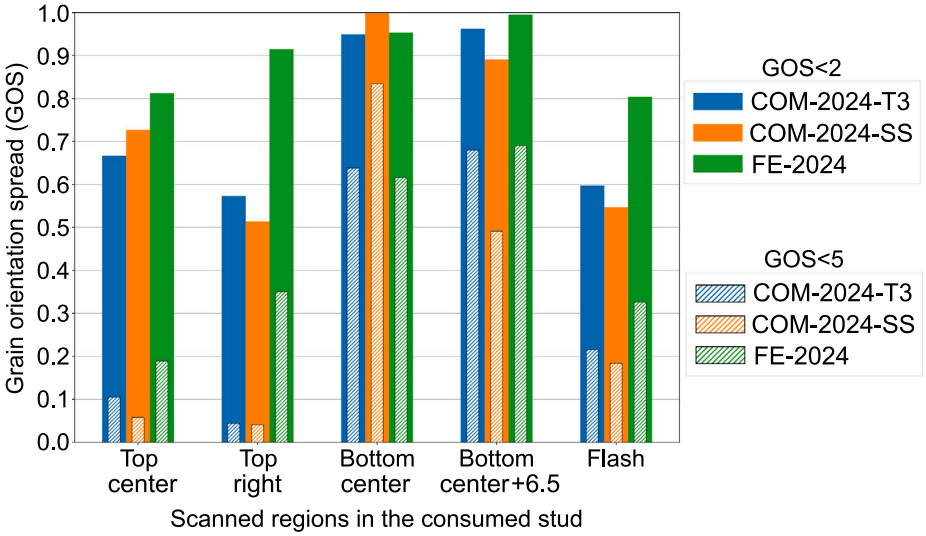

Fig. 9. Grain orientation spread (GOS) below 2° and 5° of scans of COM-2024-T3, COM-2024-SS, FE-2024 studs after friction surfacing, according to positions in Fig. 2b: top center (TC), top edge (TE), bottom center (BC), bottom center +6.5 mm (BC+6.5), flash (FL). Analyzed positions of the bottom center scans are defined by black dashed lines in the respective IPF maps in Fig. 8a.

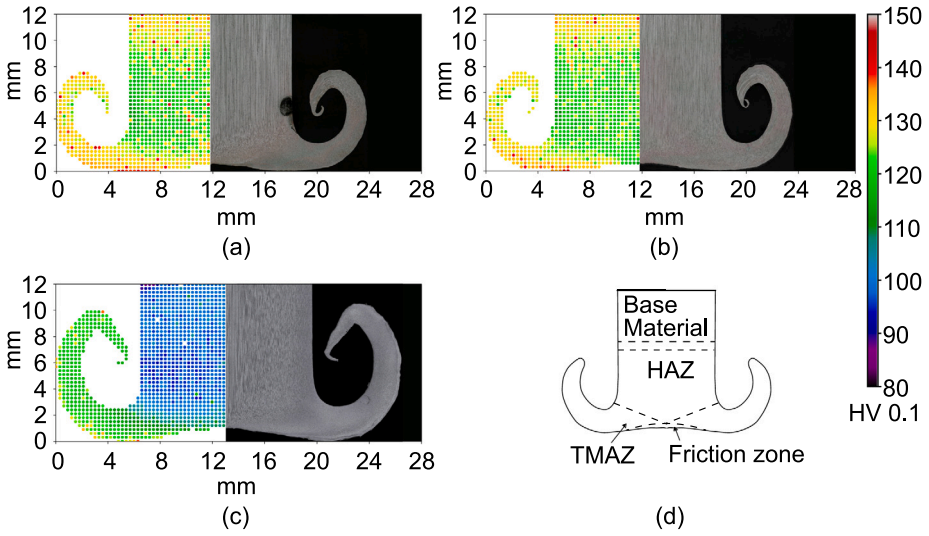

Fig. 10. Hardness map and etched cross-sections of consumed friction surfacing studs: (a) COM-2024-T3, (b) COM-2024-SS, (c) FE-2024. The point spacing between indentations is 0.3 mm along the radius and the height. (d) Schematic representation of the different process regions of the stud.

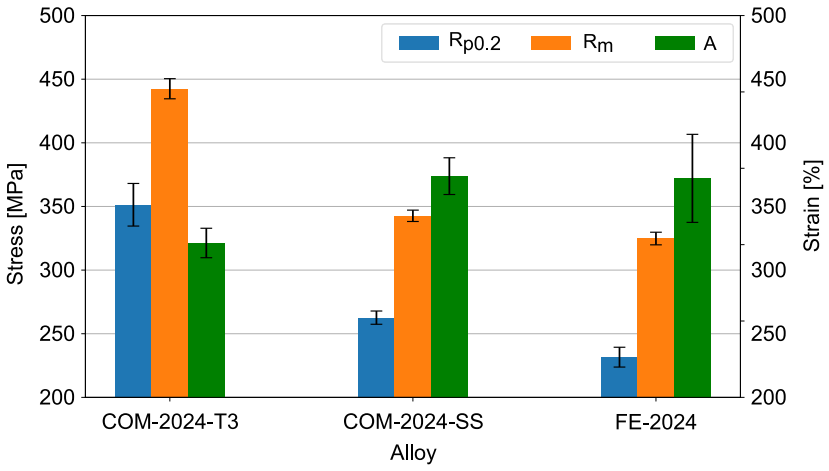

Fig. 11. Mechanical properties determined via Imprintec indentation method [42], including yielding strength ($R_{p0.2}$), ultimate tensile strength (R_m), elongation at break (A) with 1 standard deviation error bars of COM-2024-T3, COM-2024-SS and FE-2024.

features lower mechanical strength but a similar elongation at break and thus requires less energy to be deformed. The volume deposited during FS of FE studs is slightly higher compared to hot extruded consumable material. Another difference is represented by the assumed contact radius, which decreases in case of FE studs. The calculation of the assumed contact radius is affected by the deposit geometry and the stud consumption rate, Eq. (2) [44]. Using this approach, it can be observed that the different materials, i.e., conventionally extruded and FE, feature a different contact area below the respective stud, resulting in different process behavior at similar FS process parameters.

Additionally, it can be noticed that in the analysis of the studs, see Section 3.3, the initially different BM grain sizes are refined to a similar ultrafine grain size in the deposit. The mechanism of deposition was already studied in literature [51], and it is assumed that DRX occurs at different magnitudes. During FS layer deposition, the material undergoes a complex combination of different phenomena, i.e., temperature, strains and stresses, activating DRX and refining the grain size. In fact, all the analyzed studs, which experienced different consumption rates during the FS deposition, present a comparable grain size at the stud tips (BC and BC+6.5 in Fig. 8b). This indicates that a saturation of grain size is achieved. Looking at similar solid-state processing techniques like friction stir processing, similar results are reported when performing multi-pass processing [59,60]. In these studies, a second and third pass did not lead to significant further grain refinement.

All the above findings lead to the conclusion that a finer microstructure affects the FS process behavior in almost all of its aspects, and a different set of parameters would be required to achieve a similar process behavior. The deposits present a slightly different geometry; however, significant effects on the final microstructure of the deposits could not be identified, indicating a similar dynamic recrystallization mechanism. Furthermore, this study has shown that the deposition of FE studs via friction surfacing is successfully possible, providing a new pathway in terms of depositing tailored compositions and microstructures. In this regard, the results present some guidelines on how to handle different stud microstructures for coating applications as well as solid-state additive manufacturing.

4. Summary and conclusions

For the first time, the successful deposition of friction extruded studs via friction surfacing is presented, demonstrating a promising alternative to current fusion-based AM techniques. A comparison of friction extruded with conventional (hot extruded) consumable material in as-processed and solid solutionized conditions is performed.

The results provide a deeper understanding of the significance of the consumable stud microstructure for the FS process. The main findings can be summarized as follows:

- At similar process parameters, the friction extruded consumable material presents a 81% higher feed rate compared to conventional hot extruded consumable stud material during FS layer deposition.
- The deposits microstructure is similar for all AA2024 consumable materials investigated, with a ultrafine grain size of 1.4 μm.
- The microstructure and hardness at the tip of the consumed stud are independent of the extrusion process, showing an ultrafine grain size of 1.3–1.5 μm, for hot extruded and friction extruded studs, respectively, and a hardness in the range of 120–130 HV0.1.

Overall, friction extrusion can be an alternative production route for FS consumable studs, unlocking the potential of using recycled or newly tailored chemical compositions for solid-state additive manufacturing. However, careful consideration of FS process parameters is essential as the process behavior differs from conventional (hot extruded) stud material. Future research could focus on multi-layer friction surfacing to assess the feasibility of additive manufacturing. Additionally, the deposits of friction extruded studs from recycled material and/or tailored chemical compositions represent the next steps in establishing this solid-state processing route.

CRediT authorship contribution statement

Pietro Aspes: Writing – review & editing, Writing – original draft, Visualization, Validation, Methodology, Investigation, Formal analysis, Data curation. **Zina Kallien:** Writing – review & editing, Writing – original draft, Visualization, Methodology, Investigation, Formal analysis, Data curation, Conceptualization. **Lars Rath:** Writing – review & editing, Methodology. **Uceu Suhuddin:** Writing – review & editing, Methodology, Investigation. **Benjamin Klusemann:** Writing – review & editing, Supervision, Resources, Funding acquisition.

Funding

This project has received funding from the European Research Council (ERC) under the European Unions Horizon 2020 research and innovation programme (Grant Agreement No. 101001567).

Declaration of competing interest

The authors declare that they have no known competing financial interests or personal relationships that could have appeared to influence the work reported in this paper.

Appendix A. Inverse pole figure maps of friction surfacing depositions

Fig. A.12 shows the IPF maps used to obtain the grain sizes of the FS depositions.

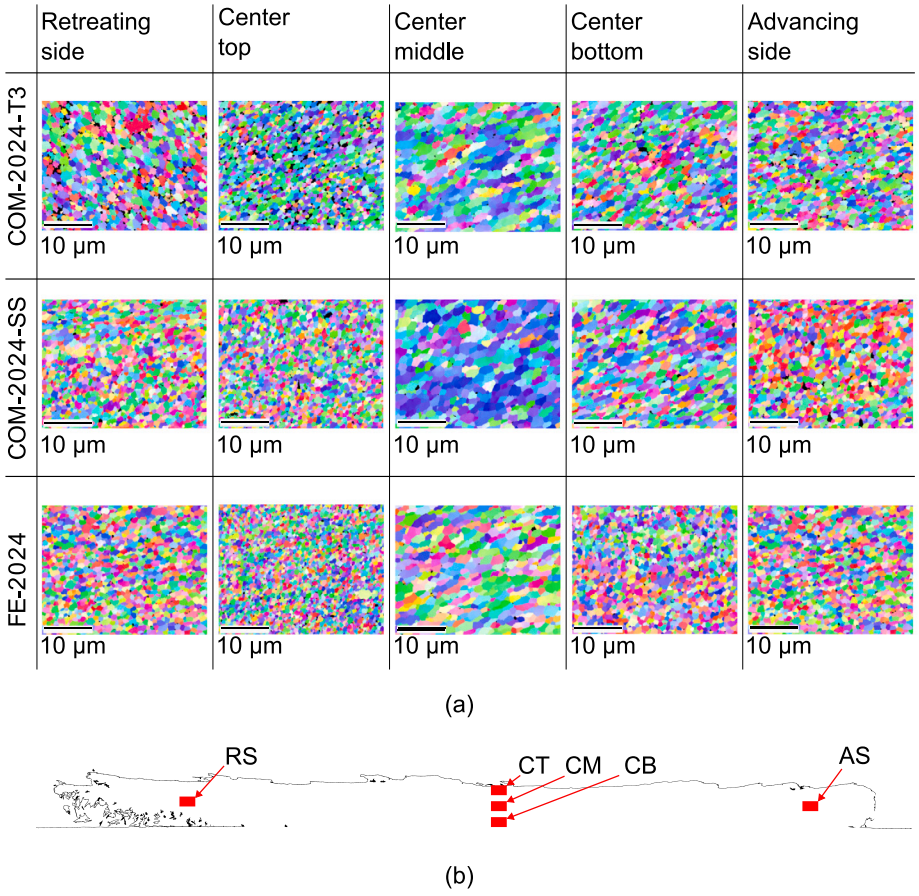

Fig. A.12. (a) Inverse pole figure maps of COM-2024-T3, COM-2024-SS and FE-2024. The scanned regions are advancing side (AS), center top (CT), center middle (CM), center bottom (CB) and retreating side (RS). (b) COM-2024-T3 reference layer image for the scanned regions.

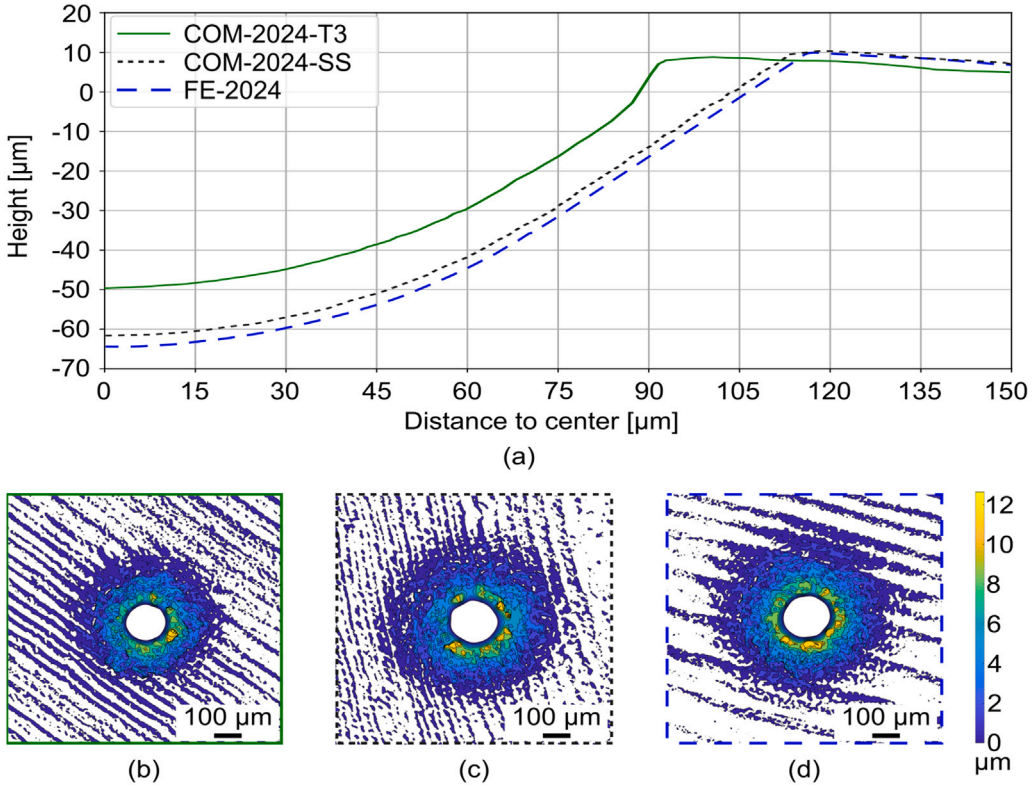

Fig. B.13. (a) Vertical profiles from the center of the Imprintec indentations on the surface of COM-2024-SS and FE-2024. Corresponding pile-up maps of indentations of (b) COM-2024-T3, (c) COM-2024-SS, (d) FE-2024.

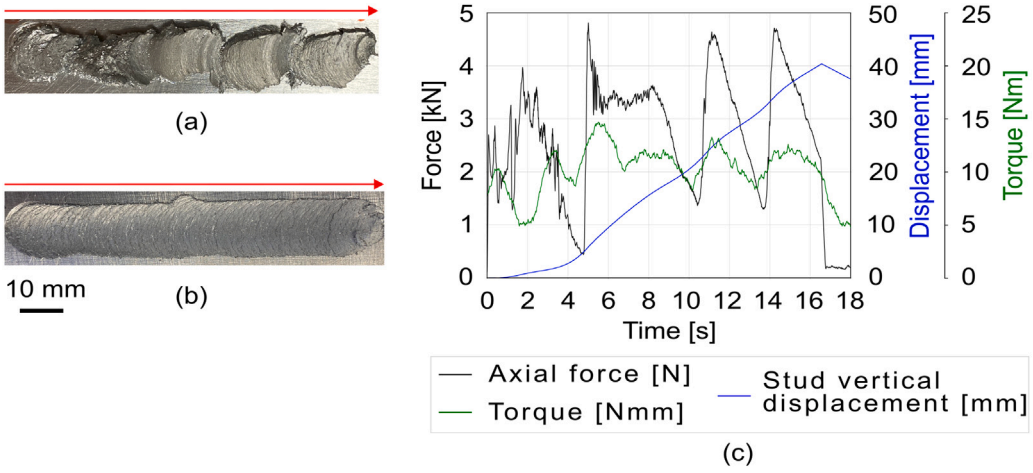

Fig. C.14. Top view of deposits: (a) COM-2024-O and (b) COM-2024-T4. The arrow represents the advancing side and points from the beginning to the end of the deposition process. (c) Process behavior of the friction surfacing deposition phase of COM-2024-O, indicating an unstable process behavior.

Appendix B. Hardness indentation profiles

Fig. B.13 shows the profiles of the performed Imprintec indentations, where the results are presented in Fig. 11. It is important to note that the HV of COM-2024-SS and FE-2024 is comparable, while COM-2024-T3 features a higher value. The maximum depth changes according to the hardness value of the tested material, and very similar values can be recognized for FE-2024 and COM-2024-SS. The same applies to the distance of highest peak to center of the indentation, where FE-2024 and COM-2024-SS show very similar values.

Appendix C. Results for T4 and O temper of conventional (hot extruded) AA2024

In addition to the heat treatments presented above for the conventional (hot extruded) AA2024 consumable material, the temper states O (COM-2024-O) and T4 (COM-2024-T4) were also investigated, see Table C.5. Layer pictures are presented in Fig. C.14, and studs image in Fig. C.15. The COM-2024-O sample presented a very unstable deposition process, Fig. C.14c. The force cannot be stabilized during the process and, consequently, the vertical displacement of the stud is not linear and the thickness of the deposit is very inhomogeneous. Additionally, the COM-2024-O stud features a very uncommon shape

Fig. C.15. Light-optical micrographs of cross-section studs after the friction surfacing deposition process: (a) COM-2024-O, representing an uncommon shape the consumed FS after deposition, (b) COM-2024-T4, featuring a typical FS stud after the deposition.

Table C.5
Overview of O and T4 consumable materials and respective heat treatments used for conventional (hot extruded) AA2024.

Label	Description
COM-2024-T4	conventional hot extruded AA2024-T3 solid solution treated (as above) followed by 10 days of natural aging prior to the FS process
COM-2024-O	conventional hot extruded AA2024-T3 with 2.5 h exposure to 410 °C in the furnace without salts bath followed by room temperature in air cooling

Table C.6
Friction surfacing process average (AVG) torque and consumption rate of the stud during deposition (steady-state conditions) and hardness of the respective consumable stud base material.

Process	AVG torque, (Nm)	AVG consumption rate, (mm/s)	BM hardness, (HV0.1)
COM-2024-O	11.14	2.99	94
COM-2024-T4	11.27	1.18	144

for FS, Fig. C.15a. It is assumed that its formation is caused by a very unstable force during the deposition at non-optimized process parameters for this temper state. The BM hardness of COM-2024-T4 is very similar to BM COM-2024-T3. The deposition behavior of these two samples was very similar, comparing Tables 3 and C.6.

Data availability

The obtained data of this research is online available at Zenodo (https://doi.org/10.5281/zenodo.15234183).

References

[1] E.A. Olivetti, J.M. Cullen, Toward a sustainable materials system, Science 360 (6396) (2018) 1396–1398, http://dx.doi.org/10.1126/science.aat6821.
[2] E. Sevigné-Itoiz, C.M. Gasol, J. Rieradevall, X. Gabarrell, Environmental consequences of recycling aluminum old scrap in a global market, RCR Adv. 89 (2014) 94–103, http://dx.doi.org/10.1016/j.resconrec.2014.05.002.
[3] A.E. Tekkaya, V. Güley, M. Haase, A. Jäger, Hot Extrusion of Aluminum Chips, in: ICAA13, John Wiley & Sons Ltd, 2012, pp. 1559–1573, http://dx.doi.org/10.1002/9781118495292.ch235.
[4] X. Li, A. Reynolds, C. Baoqiang, D. Jialuo, S. Williams, Production and properties of a wire-arc additive manufacturing part made with friction extruded wire, in: TMS 2015 144th Annual Meet. & Exhib.: Suppl. Proc., 2016, pp. 445–452, http://dx.doi.org/10.1007/978-3-319-48127-2_56.
[5] G. Carvalho, G. Campatelli, L. Fratini, Feasibility study of using friction stir extruded recycled aluminum rods for welding and additive manufacturing, Manuf. Lett. 42 (2024) 52–55, http://dx.doi.org/10.1016/j.mfglet.2024.10.007.
[6] B. Wan, W. Chen, T. Lu, F. Liu, Z. Jiang, M. Mao, Review of solid state recycling of aluminum chips, RCR Adv. 125 (2017) 37–47, http://dx.doi.org/10.1016/j.resconrec.2017.06.004.
[7] M. Reza-E-Rabby, T. Wang, N. Canfield, T. Roosendaal, B.S. Taysom, D. Graff, D. Herling, S. Whalen, Effect of various post-extrusion tempering on performance of AA2024 tubes fabricated by shear assisted processing and extrusion, CIRP J. Manuf. Sci. Technol. 37 (2022) 454–463, http://dx.doi.org/10.1016/j.cirpj.2022.02.025.
[8] G. Faraji, M.M. Mashhadi, H.S. Kim, Tubular channel angular pressing (tcap) as a novel severe plastic deformation method for cylindrical tubes, Mater. Lett. 65 (19) (2011) 3009–3012, http://dx.doi.org/10.1016/j.matlet.2011.06.039.
[9] E.A. Gadallah, H.H. El-fahhar, M.M.Z. Ahmed, M.M. El Sayed Seleman, B. Alzahrani, A.A. Alamry, Aliand El Aty, E. El Shrief, Experimental study and finite element modelling of pure copper tube fabrication via the parallel tubular channel angular pressing (ptcap) process, Mater. Res. Express (2024) http://dx.doi.org/10.1088/2053-1591/ad37a4.
[10] M. Kawasaki, Z. Horita, T.G. Langdon, Microstructural evolution in high purity aluminum processed by ecap, Mater. Sci. Eng. A 524 (1–2) (2009) 143–150, http://dx.doi.org/10.1016/j.msea.2009.06.032.
[11] Y. Ivanisenko, R. Kulagin, V. Fedorov, A. Mazilkin, T. Scherer, B. Baretzky, H. Hahn, High pressure torsion extrusion as a new severe plastic deformation process, Mater. Sci. Eng. A 664 (2016) 247–256, http://dx.doi.org/10.1016/j.msea.2016.04.008.
[12] M.E. Mehtedi, A. Forcellese, T. Mancia, M. Simoncini, S. Spigarelli, A new sustainable direct solid state recycling of AA1090 aluminum alloy chips by means of friction stir back extrusion process, Proc. CIRP 79 (2019) 638–643, http://dx.doi.org/10.1016/j.procir.2019.02.062.
[13] W. Tang, A. Reynolds, Production of wire via friction extrusion of aluminum alloy machining chips, J. Mater. Process. Technol. 210 (15) (2010) 2231–2237, http://dx.doi.org/10.1016/j.jmatprotec.2010.08.010.
[14] S.K. Das, J.G. Kaufman, Recycling aluminum aerospace alloys, Adv. Mater. Process. 166 (3) (2008) 34.
[15] G. Buffa, D. Campanella, M. Adnan, U. La Commare, G. Ingarao, L. Fratini, Improving the industrial efficiency of recycling aluminum alloy chips using friction stir extrusion: Thin wires production process, Int. J. Precis. Eng. Manuf.-Green Technol. (2024) http://dx.doi.org/10.1007/s40684-023-00573-w.
[16] T. Wang, X. Li, Z. Li, T. Liu, X. Wang, A. Devaraj, C.A. Powell, J.F. dos Santos, Upcycled high-strength aluminum alloys from scrap through solid-phase alloying, Nat. Comm. 15 (1) (2024) 10664, http://dx.doi.org/10.1038/s41467-024-53062-2.
[17] S. Whalen, M. Olszta, C. Roach, J. Darsell, D. Graff, M. Reza-E-Rabby, T. Roosendaal, W. Daye, T. Pelletiers, S. Mathaudhu, N. Overman, High ductility aluminum alloy made from powder by friction extrusion, Mater. 6 (2019) 100260, http://dx.doi.org/10.1016/j.mtla.2019.100260.
[18] M. Song, J. Darsell, S. Jana, Amorphization and alloying in Al-Ti system through friction extrusion method, J. Mater. Sci. 57 (25) (2022) 12055–12063, http://dx.doi.org/10.1007/s10853-022-07355-w.
[19] O.D. Neikov, Mech. Alloy. (2019) 91–124, http://dx.doi.org/10.1016/B978-0-08-100543-9.00003-8.
[20] Z. Feng, S. David, V. Manchiraju, D. Ferderick, W. Thomas, Friction extrusion: Solid-state metal synthesis and recycling in sustainable manufacturing, JOM 75 (2023) 2962–2973, http://dx.doi.org/10.1007/s11837-023-05824-4.
[21] G. Buffa, D. Campanella, F. Micari, L. Fratini, Design and development of a new machine tool for continuous friction stir extrusion, CIRP J. Manuf. Sci. Technol. 41 (2023) 391–400, http://dx.doi.org/10.1016/j.cirpj.2023.01.004.
[22] V. Yakubov, H. Ostergaard, S. Bhagavath, C.L.A. Leung, J. Hughes, E. Yasa, M. Khezri, S.K. Löschke, Q. Li, A.M. Paradowska, Recycled aluminium feedstock in metal additive manufacturing: A state of the art review, Heliyon (2024) http://dx.doi.org/10.1016/j.heliyon.2024.e27243.
[23] T. Bor, M. De Leede, F. Deunk, J. Lind, W. Lievestro, H.-J. Smit, R. Ariës, V. Dolas, N. Helthuis, M. Luckabauer, et al., Friction screw extrusion additive manufacturing of an Al-Mg-Si alloy, Addit. Manuf. 72 (2023) 103621, http://dx.doi.org/10.1016/j.addma.2023.103621.
[24] S. Beck, C. Williamson, R. Kinser, B. Rutherford, M. Williams, B. Phillips, K. Doherty, P. Allison, J. Jordon, Examination of microstructure and mechanical properties of direct additive recycling for Al-Mg-Mn alloy Machine chip waste, Mater. Des. 228 (2023) 111733, http://dx.doi.org/10.1016/j.matdes.2023.111733.
[25] J. Wang, Y. Xie, X. Meng, Y. Zhao, S. Sun, J. Li, J. Chen, H. Chen, X. Ma, N. Wang, Y. Huang, Wire-based friction stir additive manufacturing towards isotropic high-strength-ductility Al-Mg alloys, Virtual Phys. Prototyp. 19 (1) (2024) e2417369, http://dx.doi.org/10.1080/17452759.2024.2417369.

[26] W. Dong, X. Meng, Y. Xie, X. Zhang, Z. Zhang, X. Sun, R. Guo, H. Tian, Y. Huang, Wire-feeding friction stir welding for large-gap width tolerances, Sci. Technol. Weld. Join. 29 (4) (2024) 291–295, http://dx.doi.org/10.1177/13621718241264781.

[27] A. Hassan, M. Awang, S.R. Pedapati, K. Altaf, R.V. Marode, S.W. Ahmed, Experimental investigation on tool pin profile for defect-free multi-layered laminates using friction stir additive manufacturing, Results Eng. 20 (2023) 101516, http://dx.doi.org/10.1016/j.rineng.2023.101516.

[28] Z. Shen, M. Zhang, D. Li, X. Liu, S. Chen, W. Hou, Y. Ding, Z. Sun, Y. Su, W. Li, Y. Tian, Microstructural characterization and mechanical properties of AlMg alloy fabricated by additive friction stir deposition, Int. J. Adv. Manuf. Technol. 125 (5–6) (2023) 2733–2741, http://dx.doi.org/10.1007/s00170-023-10952-x.

[29] A. Mukhopadhyay, P. Saha, A critical review on process metrics–microstructural evolution–process performance correlation in additive friction stir deposition (AFS-D), J. Braz. Soc. Mech. Sci. Eng. 44 (9) (2022) 422, http://dx.doi.org/10.1007/s40430-022-03729-y.

[30] B. Phillips, C. Mason, S. Beck, D. Avery, K. Doherty, P. Allison, J. Jordon, Effect of parallel deposition path and interface material flow on resulting microstructure and tensile behavior of Al-Mg-Si alloy fabricated by additive friction stir deposition, J. Mater. Process. Technol. 295 (2021) 117169, http://dx.doi.org/10.1016/j.jmatprotec.2021.117169.

[31] J. Gandra, H. Krohn, R. Miranda, P. Vilaça, L. Quintino, J. Dos Santos, Friction surfacing—A review, J. Mater. Process. Technol. 214 (5) (2014) 1062–1093, http://dx.doi.org/10.1016/j.jmatprotec.2013.12.008.

[32] N.A. Alsaleh, M.M. El-Sayed Seleman, A.M.M. Hassan, M.M.Z. Ahmed, S. Ataya, F.H. Latief, A. Abdul-Latif, M.I.A. Habba, Additively manufactured parts from AA2011-T6 large-diameter feedstocks using friction stir deposition, Mater. 16 (14) (2023) 4904, http://dx.doi.org/10.3390/ma16144904.

[33] S. Hanke, J.F. dos Santos, Comparative study of severe plastic deformation at elevated temperatures of two aluminium alloys during friction surfacing, J. Mater. Process. Technol. 247 (2017) 257–267, http://dx.doi.org/10.1016/j.jmatprotec.2017.04.021.

[34] Z. Kallien, L. Rath, A. Roos, B. Klusemann, Application of friction surfacing for solid state additive manufacturing of cylindrical shell structures, Addit. Manuf. Lett. (2023) 100184, http://dx.doi.org/10.1016/j.addlet.2023.100184.

[35] M. Hoffmann, A. Roos, B. Klusemann, Investigation of microstructural and mechanical properties in AA2024-T351 multi-layer friction surfacing, Surf. Coat. Technol. 480 (2024) 130610, http://dx.doi.org/10.1016/j.surfcoat.2024.130610.

[36] R.M. Halak, L. Rath, U.F.H.R. Suhuddin, J.F. Dos Santos, B. Klusemann, Changes in processing characteristics and microstructural evolution during friction extrusion of aluminum, Int. J. Mater. Form. 15 (3) (2022) 24, http://dx.doi.org/10.1007/s12289-022-01670-y.

[37] X. Li, W. Tang, A.P. Reynolds, W.A. Tayon, C.A. Brice, Strain and texture in friction extrusion of aluminum wire, J. Mater. Process. Technol. 229 (2016) 191–198, http://dx.doi.org/10.1016/j.jmatprotec.2015.09.012.

[38] M. Liang, L. Chen, G. Zhao, Y. Guo, Effects of solution treatment on the microstructure and mechanical properties of naturally aged EN AW 2024 Al alloy sheet, J. Alloys Compd. 824 (2020) 153943, http://dx.doi.org/10.1016/j.jallcom.2020.153943.

[39] H.K. Rafi, G.J. Ram, G. Phanikumar, K.P. Rao, Friction surfaced tool steel (h13) coatings on low carbon steel: A study on the effects of process parameters on coating characteristics and integrity, Surf. Coat. Technol. 205 (1) (2010) 232–242, http://dx.doi.org/10.1016/j.surfcoat.2010.06.052.

[40] G. Chen, K. Wu, Y. Wang, Y. Sun, X. Wang, Z. Zhu, F. Hu, Quantitative study on the correlation between microstructure and mechanical properties of additive friction stir deposited 6061-T6 Al-Mg-Si alloy, J. Mater. Res. Technol. 25 (2023) 6725–6736, http://dx.doi.org/10.1016/j.jmrt.2023.07.097.

[41] C.D. Barrett, A. Imandoust, A.L. Oppedal, K. Inal, M.A. Tschopp, H. El Kadiri, Effect of grain boundaries on texture formation during dynamic recrystallization of magnesium alloys, Acta Mater. 128 (2017) 270–283, http://dx.doi.org/10.1016/j.actamat.2017.01.063.

[42] B. Schmaling, A. Hartmaier, Determination of plastic material properties by analysis of residual imprint geometry of indentation, J. Mater. Res. 27 (16) (2012) 2167–2177, http://dx.doi.org/10.1557/jmr.2012.212.

[43] J. Gandra, R.M. Miranda, P. Vilaça, Performance analysis of friction surfacing, J. Mater. Process. Technol. 212 (8) (2012) 1676–1686, http://dx.doi.org/10.1016/j.jmatprotec.2012.03.013.

[44] K. Fukakusa, On the characteristics of the rotational contact plane - a fundamental study of friction surfacing, Weld. Int. 10 (7) (1996) 524–529, http://dx.doi.org/10.1080/09507119609549043.

[45] Z. Kallien, M. Hoffmann, A. Roos, B. Klusemann, Correlation of microstructure and local mechanical properties along build direction for multi-layer friction surfacing of aluminum alloys, JOM (2023) http://dx.doi.org/10.1007/s11837-023-06046-4.

[46] P. Pirhayati, H. Jamshidi Aval, Microstructural characterization and mechanical properties of friction surfaced AA2024-AG composites, Trans. Nonferr. Met. Soc. China 30 (7) (2020) 1756–1770, http://dx.doi.org/10.1016/S1003-6326(20)65336-5.

[47] J. Ehrich, A. Roos, B. Klusemann, S. Hanke, Influence of Mg content in Al alloys on processing characteristics and dynamically recrystallized microstructure of friction surfacing deposits, Mater. Sci. Eng. A 819 (2021) 141407, http://dx.doi.org/10.1016/j.msea.2021.141407.

[48] Z. Rahmati, H. Jamshidi Aval, S. Nourouzi, R. Jamaati, Effect of friction surfacing parameters on microstructure and mechanical properties of solid-solutionized AA2024 aluminium alloy cladded on AA1050, Mater. Chem. Phys. 269 (2021) 124756, http://dx.doi.org/10.1016/j.matchemphys.2021.124756.

[49] Z. Rahmati, H. Jamshidi Aval, S. Nourouzi, R. Jamaati, Microstructural, tribological, and texture analysis of friction surfaced Al-Mg-Cu clad on AA1050 alloy, Surf. Coat. Technol. 397 (2020) 125980, http://dx.doi.org/10.1016/j.surfcoat.2020.125980.

[50] M. Hoffmann, Z. Kallien, E. Antunes Duda, B. Klusemann, Insight into layer formation during friction surfacing: Relationship between deposition behavior and microstructure, Mater. Today Commun. (2024) 110337, http://dx.doi.org/10.1016/j.mtcomm.2024.110337.

[51] U. Suhuddin, S. Mironov, H. Krohn, M. Beyer, J.F. Dos Santos, Microstructural evolution during friction surfacing of dissimilar aluminum alloys, Metall. Mater. Trans. A 43 (13) (2012) 5224–5231, http://dx.doi.org/10.1007/s11661-012-1345-8.

[52] K. Huang, R.E. Logé, A review of dynamic recrystallization phenomena in metallic materials, Mater. Des. 111 (2016) 548–574, http://dx.doi.org/10.1016/j.matdes.2016.09.012.

[53] C.J.D. Santiagu, D. Ramachandran, M.K. Gangaraju, K.R. Sajja Rama, Friction deposition additive manufacturing of alloy 718: Effect of post-heat treatment on microstructures and mechanical properties, Int. J. Adv. Manuf. Technol. 128 (9) (2023) 3901–3919, http://dx.doi.org/10.1007/s00170-023-12141-2.

[54] P. Pirhayati, H.J. Aval, An investigation on thermo-mechanical and microstructural issues in friction surfacing of Al–Cu aluminum alloys, Mater. Res. Express 6 (5) (2019) 056550, http://dx.doi.org/10.1088/2053-1591/ab0635.

[55] N.Q. Chinh, P. Szommer, Z. Horita, T.G. Langdon, Experimental evidence for grain-boundary sliding in ultrafine-grained aluminum processed by severe plastic deformation, Adv. Mater. 18 (1) (2006) 34–39, http://dx.doi.org/10.1002/adma.200501232.

[56] M.B. Lezaack, F. Hannard, A. Simar, Understanding the ductility versus toughness and bendability decoupling of large elongated and fine grained Al 7475 - T6 alloy, Mater. Sci. Eng. A 839 (2022) 142816, http://dx.doi.org/10.1016/j.msea.2022.142816.

[57] M.M.Z. Ahmed, M.M. El-Sayed Seleman, E. Elfishawy, B. Alzahrani, K. Touileb, M.I.A. Habba, The effect of temper condition and feeding speed on the additive manufacturing of AA2011 parts using friction stir deposition, Mater. (Basel) 14 (21) (2021) http://dx.doi.org/10.3390/ma14216396.

[58] Z. Kallien, A. Roos, C. Knothe-Horstmann, B. Klusemann, Temperature-dependent mechanical behavior of aluminum AM structures generated via multi-layer friction surfacing, Mater. Sci. Eng. A 871 (2023) 144872, http://dx.doi.org/10.1016/j.msea.2023.144872.

[59] Y. Chen, H. Ding, J. Li, Z. Cai, J. Zhao, W. Yang, Influence of multi-pass friction stir processing on the microstructure and mechanical properties of Al-5083 alloy, Mater. Sci. Eng. A 650 (2016) 281–289, http://dx.doi.org/10.1016/j.msea.2015.10.057.

[60] R. Brown, W. Tang, A. Reynolds, Multi-pass friction stir welding in alloy 7050-T7451: Effects on weld response variables and on weld properties, Mater. Sci. Eng. A 513- 514 (2009) 115–121, http://dx.doi.org/10.1016/j.msea.2009.01.041.